View Journal

# Catalysis Science & Technology

Accepted Manuscript

This article can be cited before page numbers have been issued, to do this please use: H. Jahnagiri, A. Osatiashtiani, J. Bennett, M. A. Isaacs, S. Gu, A. F. Lee and W. Karen, *Catal. Sci. Technol.*, 2018, DOI: 10.1039/C7CY02541F.




ROYAL SOCIETY OF CHEMISTRY

rsc.li/catalysis

DOI: 10.1039/C7CY02541F

Journal Name

ARTICLE

# Zirconia catalysed acetic acid ketonisation for pre-treatment of biomass fast pyrolysis vapours.

Received 00th January 20xx,
Accepted 00th January 20xx

DOI: 10.1039/x0xx00000x

www.rsc.org/

Hessam Jahangiri,[a,b] Amin Osatiashtiani,[a] James A. Bennett,[a] Mark A. Isaacs,[a] Sai Gu,[c] Adam. F. Lee[d] and Karen Wilson*[d]

Crude pyrolysis bio-oil contains significant quantities of carboxylic acids which limit its utility as a biofuel. Vapour phase ketonisation of organic acids contained within biomass fast-pyrolysis vapours offers a potential pre-treatment to improve the stability and energy content of resulting bio-oils formed upon condensation. Zirconia is a promising catalyst for such reactions, however little is known regarding the impact of thermal processing on the physicochemical properties of zirconia in the context of their corresponding reactivity for the vapour phase ketonisation of acetic acid. Here we show that calcination progressively transforms amorphous $Zr(OH)_4$ into small tetragonal $ZrO_2$ crystallites at 400 °C, and subsequently larger monoclinic crystallites >600 °C. These phase transitions are accompanied by an increase in the density of Lewis acid sites, and concomitant decrease in their acid strength, attributed to surface dehydroxylation and anion vacancy formation. Weak Lewis acid sites (and/or resulting acid-base pairs) are identified as the active species responsible for acetic acid ketonisation to acetone at 350 °C and 400 °C, with stronger Lewis acid sites favouring competing unselective reactions and carbon laydown. Acetone selectivity is independent of acid strength.

## Introduction

Concerns over energy security and demand, and the parallel impact of $CO_2$ emissions from fossil fuels on global warming are driving a quest to find sustainable low carbon energy sources.[1, 2] Waste lignocellulosic (non-edible) biomass is the only sustainable hydrocarbon source that can provide an immediate environmentally-benign replacement for non-renewable liquid transportation fuels.[2] However, such biomass-derived fuels are currently incompatible with existing distribution infrastructure and vehicle engines, and require catalytic upgrading to improve their physicochemical properties prior to implementation.[3, 4]

Bio-oil production by fast pyrolysis[5, 6], hydrothermal liquefaction,[7, 8] or gasification[9] and subsequent Fischer–Tropsch synthesis,[10,11] are the main thermochemical technologies to convert lignocellulosic biomass into liquid hydrocarbons. Fast pyrolysis bio-oils are complex mixtures of oxygenated compounds comprising phenolics, furanics, carboxylic acids and other small oxygenates, the composition of which depends on biomass source and processing conditions.[6, 12, 13] The high oxygen content of crude bio-oil results in a heating value half that of petroleum-derived fuels, while the presence of carboxylic acids and small reactive oxygenates (e.g. unsaturated aldehydes) renders the oils corrosive (pH 2-3)[13] and chemically unstable.[3] Crude bio-oils must therefore be upgraded to remove corrosive components and stabilise them prior to any final hydrodeoxygenation step to enhance their calorific value.

Ketonisation,[14-16] involving the condensation of two acid molecules to form a ketone, $CO_2$ and $H_2O$ (**Scheme 1**), and esterification[17-19] involving the reaction of carboxylic acids with alcohols (already present or from external addition), are promising routes to lower the acidity of crude bio-oil. Ketonisation is advantageous since it can be conducted in the vapor phase without additional reactants, thereby enabling a catalyst bed close-coupled to the fast pyrolysis unit to remove acids from pyrolysis vapour prior to condensation as a bio-oil.[16, 20] In addition to reducing acidity, ketonisation also results in bio-oil deoxygenation and concomitant hydrocarbon chain growth.[21]

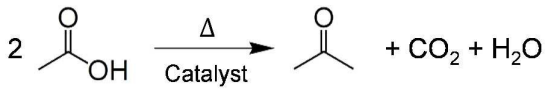


Scheme 1. Acetic acid ketonisation.

Ketonisation is an established reaction in organic synthesis,[20, 22] which can take place over various polycrystalline oxides including alkali earth metal oxides (e.g. MgO, $BaO$[23, 24]), transition metal oxides (e.g. $CeO_2$[25, 26], $MnO_2$[16, 27, 28], $TiO_2$[29, 30], $Fe_3O_4$[14, 16, 31] and $ZrO_2$[32, 33]), and actinide oxides (e.g. $ThO_2$[34]). Mixed oxides of Ni, Co and Cu[23] and layered double hydroxides of Zn/Al and Mg/Al have also been explored for carboxylic acid ketonisation.[35, 36] Promising results have been reported for

[a] European Bioenergy Research Institute, Aston University, Birmingham B4 7ET, UK.
[b] Cranfield University, Whittle Building, Cranfield, Bedfordshire MK43 0AL, UK.
[c] University of Surrey, Guildford, Surrey GU2 7XH, UK.
[d] School of Science, RMIT University, Melbourne VIC3000, Australia.
Email:karen.wilson2@rmit.edu.au

Electronic Supplementary Information (ESI) available: Additional structural and reactivity data. See DOI: 10.1039/x0xx00000x

View Article Online
DOI: 10.1039/C7CY02541F




$ZrO_2$, $TiO_2$, and $CeO_2$,[37-39] reflecting the presence of cationic and anionic vacancies.[20] $ZrO_2$ catalysed ketonisation may be promoted by alkali metal ion (such as $K^+$ or $Na^+$) to tune their acid/base properties.[40]

Ketonisation proceeds via two distinct pathways depending on the lattice energy of the metal oxide, with low lattice energy (strong bases) forming stable carboxylates that thermally decompose at elevated temperature (>420 °C)[41] to yield ketones, whereas high lattice energy oxides enable a lower temperature surface catalysed route.[20] Despite extensive research, mechanistic aspects of heterogeneously catalysed ketonisation are still a matter of debate.[20] Mechanisms based on Eley-Rideal[42] and Langmuir-Hinshelwood models[23, 43] have both been proposed, with the latter more widely accepted.[44] Ketonisation requires that one acid molecule possesses an α-H-atom relative to the -COOH group, with subsequent enolate formation occurring through either α-H abstraction, or α-H migration via keto-enol tautomerization. The resulting enolate is proposed to attack a second Lewis acid coordinated, monodentate acetate species to form a β-keto acid intermediate, which in turn decomposes via $CO_2$ and $H_2O$ elimination to yield the ketone product.[14, 45]

Zirconia is an attractive metal oxide for acetic acid ketonisation, owing to its corrosion resistance, amphoteric properties, and ability to stabilise undercoordinated cations necessary for carboxylic acid coordination.[40, 46] The phase and surface termination of zirconia may also be readily tuned to optimise its corresponding surface chemistry and catalytic activity/selectivity. Recent studies suggest that ketonisation proceeds over zirconia via carboxylic acid adsorption in a monodentate conformation at coordinatively unsaturated Zr-O pairs, with mildly basic $O^{2-}$ sites promoting α-H abstraction and enolate formation. Enolates subsequently couple with acetic acid molecularly chemisorbed at an adjacent $Zr^{4+}$ Lewis site.[20, 47] Monoclinic $ZrO_2$ exhibits a higher turnover rate (normalised per acid-base pair) compared to the tetragonal phase, attributed to its enhanced basicity.[45] However, the monoclinic phase undergoes rapid deactivation, possibly due to facile deprotonation of carboxylic acids and the attendant formation of inert bidentate carboxylates at Zr-O-Zr sites.[47] Although mechanistic studies suggest that the higher basicity of $O^{2-}$ in monoclinic zirconia should promote the critical α-H cleavage, such strong basic sites are also more likely to deactivate on-stream under mild reaction conditions (<400 °C) due to adsorption of reactively-formed $CO_2$.[48] Despite these reports, the relationship between Lewis acidity and ketonisation activity and selectivity over different $ZrO_2$ polymorphs remains poorly established.

Herein we report on the relationship between the surface chemistry of tetragonal and monoclinic zirconia, notably acid strength and site density, and reactivity for the continuous vapour phase ketonisation of acetic acid to acetone.

## Experimental

### Catalyst preparation

Zirconium hydroxide $Zr(OH)_4$ (MEL Chemicals XZO880/01) was calcined in static air at temperatures between 300-800 °C for 4 h, with the resulting materials named $ZrO_2$(x), where x is the calcination temperature.

### Catalyst characterisation

Phase identification was evaluated by wide angle XRD using a Bruker D8 Advance diffractometer and Cu $K_\alpha$ radiation between range 2θ = 10-80 ° with a step size of 0.04 °. The ratio between tetragonal and monoclinic phases was calculated from their principal reflections at 2θ=50.3 ° and 28.3 ° respectively, with crystallite sizes determined by Scherrer analysis of the same reflections.

Surface areas, pore size distributions and mesopore volumes were determined by $N_2$ porosimetry using a Quantasorb Nova 4000e porosimeter using Quantachrome Novawin 11.0 software. Samples were outgassed in vacuo at 120 °C for 2 h prior to analysis, with specific surface areas calculated by applying the Brunauer–Emmet–Teller (BET) model over the range $P/P_0$ = 0.05-0.30 of the isotherm. Pore size distributions and mesopore volumes were calculated by applying the Barrett–Joyner–Halenda (BJH) model to the desorption branch of the isotherm.

XPS measurements were carried out using a Kratos Axis HSi photoelectron spectrometer equipped with a charge neutraliser and a Mg $K_\alpha$ X-ray source (hν = 1253.6 eV). Spectra were recorded using an analyser pass energy of 20 eV and X-ray power of 225 W at a normal emission. Valence band spectra were recorded on a Kratos Supra employing a monchromated Al $K_\alpha$ X-ray source (hν = 1486.7 eV). Spectral fitting was performed using CasaXPS version 2.3.14, with binding energies corrected to the C 1s peak at 284.6 eV, and high-resolution C 1s, O 1s and Zr 3d XP spectra fitted using a common Gaussian/Lorentzian line shape. Spectra were Shirley background-subtracted and surface compositions quantified by application of element and instrument specific response factors. Errors in surface composition were estimated by varying the background subtraction procedure across reasonable limits and re-calculating fits.

The carbon content of spent catalysts was measured using a Thermo Scientific Flash 2000 organic elemental analyser calibrated to sulfanilamide, fitted with a Cu/CuO CHNS quartz tube and a TCD. Samples were prepared by adding ~10 mg catalyst and ~2 mg $V_2O_5$ to tin crucibles.

Acid site loadings and strength were determined via *n*-propylamine (Sigma Aldrich, ≥99 %) temperature programmed reaction using a Mettler Toledo TGA/DSC 2 STARe system connected to a Pfeiffer Vacuum ThermoStar GSD 301 T3 Benchtop Mass Spectrometer (MS). Propylamine adsorption was performed by dosing liquid *n*-propylamine onto pre-weighed samples (1 ml/20 mg) in the TGA crucible cell. Excess physisorbed propylamine was removed by drying in a vacuum oven at 30 °C prior to sample loading in the TGA. Samples were heated in the TGA furnace from 40 °C to 800 °C at a ramp rate of 10 °C.min$^{-1}$ under flowing $N_2$ (40 ml.min$^{-1}$), with evolved gases analysed by MS to monitor the appearance of reactively formed propene over the acid sites.

View Article Online
DOI: 10.1039/C7CY02541F
Journal Name ARTICLE



DRIFT measurements of pyridine adsorption were carried out by impregnation of the diluted samples (10 wt% in KBr) with neat pyridine. Excess physisorbed pyridine was removed in a vacuum oven at 30 °C overnight prior to sample loading in the environmental cell. DRIFT spectra of the pyridine-saturated samples were recorded at room temperature under vacuum using a Nicolet Avatar 370 MCT with Smart Collector accessory, mid/near infrared source and a mercury cadmium telluride (MCT-A) photon detector at -196 °C.

### Catalytic ketonisation

Ketonisation of acetic acid was performed in a continuous flow packed-bed reactor with online GC analysis. The reactor comprised a 1 cm o.d. quartz tube, within which the catalyst bed was placed centrally and retained by quartz wool plugs. A constant catalyst bed volume of 4 $cm^3$ was used in all experiments, comprised of 200 mg of catalyst diluted with fused silica granules. The reactor tube was positioned in a temperature-programmable furnace with a thermocouple placed in contact with the catalyst bed. Acetic acid (Sigma-Aldrich, ACS reagent, ≥ 99.7 %) was fed in a down-flow fashion into the reactor using an Agilent 1260 Infinity Isocratic Pump and $N_2$ as the carrier gas (50 $ml.min^{-1}$). All reactor lines were heated to 130 °C to prevent condensation, and a 1 cm diameter metal tube packed with fused silica granules was used to ensure acetic acid vaporisation before the reactor. For product stream analysis, a Varian 3800 GC with a heated gas-sampling valve, equipped with a BR-Q PLOT column (30 m x 0.53 mm i.d.), was employed. Acetone and acetic acid were detected by flame ionisation detector (FID). The online GC was calibrated for acetic acid and acetone by injecting 50 µl of standard solutions through a switching valve. Each injection was repeated 10 times and an average peak area taken.

Acetic acid conversion, and acetone yield and selectivity, were calculated according to Equations 1-3.

$$Conversion = \frac{n_{AcOH_0} - n_{AcOH}}{n_{AcOH_0}} \times 100 \quad \textbf{Equation 1}$$

$$Selectivity = \frac{n_{Acetone}}{n_{AcOH_0} - n_{AcOH}} \times 100 \quad \textbf{Equation 2}$$

$$Yield = \frac{Selectivity \times Conversion}{100} \quad \textbf{Equation 3}$$

where $n_{AcOH_0}$ is the initial moles of acetic acid, $n_{AcOH}$ is the final moles acetic acid and $n_{Acetone}$ represents the moles of produced as acetone.

Acetone was the main product observed over all catalysts at both 350 and 400 °C. The primary by-product was identified by GC-MS (**Figure S1**) as a secondary reaction product of acetone, 1 2-propanediol 2-acetate. Other commonly observed products such as isobutene, acetaldehyde or $CH_4$ (as a primary product of acetic acid decarboxylation)[49] were detected in trace amounts (< 1 %). Blank reactions showed no acetic acid conversion without a zirconia catalyst.

## Results and Discussion

### Catalyst characterisation

The phase composition of calcined $Zr(OH)_4$ was first monitored by XRD. No crystalline phases were observed for calcination temperatures <300 °C (**Figure 1),** suggesting the presence of either amorphous zirconia or crystallites <2 nm. However, calcination at 400 °C resulted in weak reflections at 2θ=24.2 °, 28.3 °, 31.5 °, 34.3 °, 35.5 °, 40.9 °, 49.4 °, 50.2 °, 60.2 °, and 62.9 °, characteristic of the monoclinic phase (m-$ZrO_2$), and at 2θ=30.5 °, 35.2 °, 50.3 °, and 60 ° characteristic of the tetragonal phase (t-$ZrO_2$).[50] Higher calcination temperatures favoured m-$ZrO_2$. Volume-averaged crystallite sizes revealed t-$ZrO_2$ crystallites present ≤600 °C of 9-10 nm diameter, whereas m-$ZrO_2$ crystallites grew from 14.5 to 48 nm upon calcination between 400 °C and 800 °C (**Table 1**). These temperature-dependent phase changes are consistent with previous reports,ref and a consequence of the balance between the lower surface energy of t-$ZrO_2$, and higher thermodynamic stability of bulk m-$ZrO_2$.[51] For low calcination temperatures, the surface energy contribution dominates due to the small crystallite size (9 nm), which favours the tetragonal phase, whereas following higher temperature treatment the bulk lattice energy of the larger crystallites present favours the monoclinic phase; crystallite sintering promotes a phase transition from t-$ZrO_2$→m-$ZrO_2$.

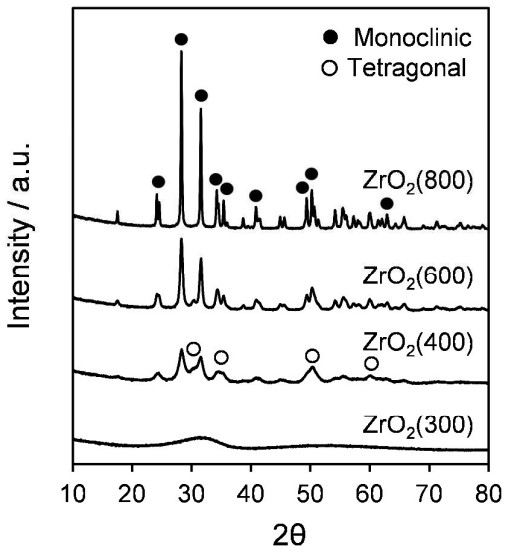


**Figure 1.** XRD patterns of $Zr(OH)_4$ as a function of calcination temperature.

Porosimetry (**Figure S2a**) reveals all $ZrO_2$ samples exhibited type IV isotherms, characteristic of mesoporous materials, attributed to the presence of interparticle voids formed during zirconia precipitation.[50] BET surface areas decreased significantly with increasing calcination temperature, consistent with $ZrO_2$ sintering into the large monoclinic crystallites observed by XRD (**Table 1**). BJH pore size distributions (**Figure S2b**) showed a concomitant increase in the size of interparticle voids.

View Article Online
DOI: 10.1039/C7CY02541F




**Table 1.** Physicochemical properties of calcined $Zr(OH)_4$.

| Catalyst | Surface area[a] / $m^2.g^{-1}$ | Avg. pore diameter[b] / nm | Crystallite size[c] / nm | | Tetragonal:monoclinic ratio[c] | O:Zr atomic ratio | Acid site loading[d] / $mmol.g^{-1}$ | Acid site density[d] / $\mu mol.m^{-2}$ | Strong:weak acid site ratio[d] |
|---|---|---|---|---|---|---|---|---|---|
| | | | Tetragonal | Monoclinic | | | | | |
| $ZrO_2$(300) | 276 | 3.4 | - | - | - | 2.7 | 0.68 | 2.5 | 34.7 |
| $ZrO_2$(400) | 190 | 3.4 | 9 | 14.5 | 0.25 | 2.3 | 0.42 | 2.2 | 5.5 |
| $ZrO_2$(600) | 38 | 5.9 | 10 | 18 | 0.11 | 2.2 | 0.13 | 3.4 | 1.4 |
| $ZrO_2$(800) | 10 | 8.0 | - | 48 | 0 | 2.2 | 0.04 | 4.0 | 1.6 |

[a]BET, [b]BJH, [c]XRD, [d]Propylamine adsorption/TGA-MS, [e]XPS.

Surface analysis (**Table 1** and **Table S1**) revealed a decrease in the surface O:Zr atomic ratio from 2.3 to 1.6 with increasing calcination temperature, ascribed to surface dehydroxylation and the creation of anion vacancies; such vacancies are essential to impart Lewis acid character to $ZrO_2$ and proposed to play a crucial role in carboxylic acid ketonisation.[15, 44, 45, 52] High-resolution O 1*s* spectra (**Figure 2a**), evidence two surface species with binding energies of 529.5 and 531.5 eV for the $ZrO_2$ (300), characteristic of $ZrO_2$ and Zr-OH respectively. Calcination increase the ratio of surface oxide:hydroxyl, consistent with surface dehydroxylation at high temperature (**Figure S3**).[53-55] The Zr 3d spin-orbit split doublet also evidenced two distinct chemical environments at 181.8 and 182.3 eV for the Zr $5d_{5/2}$ component (**Figure 2b**), attributed to $Zr^{4+}$ species in $ZrO_2$ and Zr-OH respectively, whose relative intensity increased from 0.8→2 on calcining from 300→400 °C, but was unchanged at higher temperature (again consistent with dehydroxylation). The ratio of O 1s and Zr 3d oxide components was independent of calcination temperature (**Table S1**), in accordance with the non-reducible character of large zirconia crystallites.[56] Surface dehydroxylation following calcination is also apparent from DRIFTS (**Figure S4**), wherein the 3000-3800 $cm^{-1}$ bands associated with surface hydroxyls is partially attenuated >300 °C.

Valence band XP spectra (**Figure S5**) also evidence a phase transition from amorphous $Zr(OH)_4$ to crystalline m-$ZrO_2$ after 800°C calcination, apparent as a 0.4 eV increase in the valence band energy maximum. The $ZrO_2$ valence band is comprised of hybridised O 2p and Zr 4d states, and its position and width depends on the symmetry and associated crystal field splitting of the oxide.[57] The increase in valence band energy maximum is characteristic of oxygen vacancy formation coincident with m-$ZrO_2$ high temperature crystallisation and oxygen vacancy segregation to grain boundaries,[58, 59] which open up indirect-band transitions. The generation of such vacancies and accompanying Lewis acid sites is expected to facilitate the adsorption of acetate anions.[20, 44, 60]

The nature of acid sites was subsequently probed as a function of calcination temperature by pyridine DRIFTS. **Figure S6** shows the resulting DRIFT spectra of all samples exhibit bands at 1445, 1490, and 1605 $cm^{-1}$ attributed to pyridine bound to Lewis acid sites.[50] No bands were observed at 1540 $cm^{-1}$ or 1638 $cm^{-1}$, confirming the absence of any Brønsted

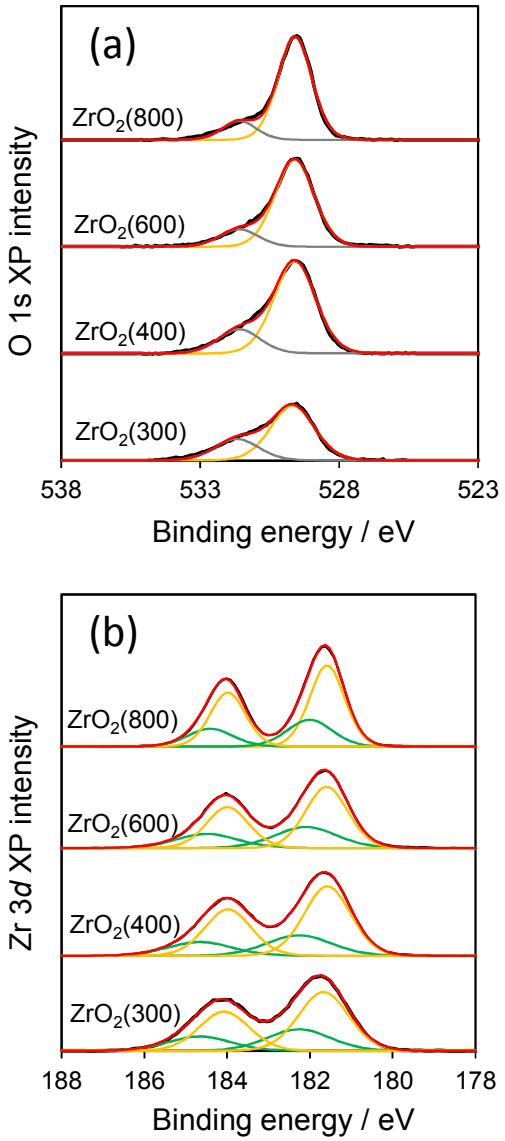


**Figure 2.** a) O 1s and b) Zr 3d spectra of $Zr(OH)_4$ as a function of calcination temperature

View Article Online
DOI: 10.1039/C7CY02541F




acidity.[61] Corresponding TPD profiles of reactively-formed propene (arising from propylamine decomposition) shown in **Figure 3** show the acid strength evolves with calcination temperature. $ZrO_2$(300) exhibited a single propene desorption ~368 °C, associated with strong acid sites, most likely originating from high-index facets or defects.[62] Higher temperature calcination resulted in the emergence of a second desorption peak at 500 °C, indicative of weaker Lewis acid sites. Acid site loadings and corresponding densities are shown in **Table 1**, and reveal that calcination increases the total acid site density (due to vacancy formation) from 2.5→4.0 μmol.m$^{-2}$, associated with the emergence of weak acid sites (**Figure S7**). The presence of weak and strong acid sites on $ZrO_2$ has previously been suggested by $NH_3$-TPD, which shows only a poorly resolved doublet desorption peak,[63] and also by using potentiometric titration.[61] While the strength of the weak acid sites remains unchanged with calcination temperature, the stronger acid sites are observed to weaken with progressive recrystallization of $ZrO_2$, evidenced by an increase in the desorption temperature of reactively-formed propene. We postulate that this weakening may reflect coupling of $Zr^{4+}$ Lewis acid sites to basic $O^{2-}$ as $Zr^{4+}$-$O^{2-}$ defect pairs.[64] This hypothesis is supported by $CO_2$ titration (**Table S2**) which reveals that calcination also increases the base site density.

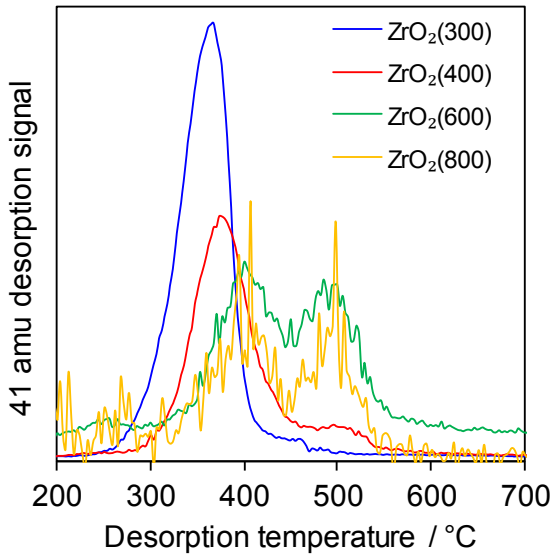


**Figure 3.** Reactively-formed propene TPD from propylamine chemisorbed over $Zr(OH)_4$ as a function of calcination temperature (normalised to surface area).

In summary, the phase transition from t- to m-$ZrO_2$ that accompanies high temperature calcination of zirconia is accompanied by surface dehydroxylation, anion vacancy formation, and the appearance of weak acid sites,[61, 65, 66 67]

### Acetic acid ketonisation

Vapour phase acetic acid ketonisation was subsequently investigated over calcined $Zr(OH)_4$ in a fixed-bed continuous flow reactor. Turnover frequencies (TOFs) normalised per acid site determined at iso-conversion for reactions at both 350 °C and 400 °C increased monotonically with calcination temperature up to 800 °C (**Figure 4**). The ratio of weak:strong acid site densities from propylamine TPD mirrors the trend in reactivity, demonstrating that ketonisation is structure-sensitive, and occurs preferentially over weak acid sites (or unsaturated $Zr^{4+}$-$O^{2-}$ acid-base pairs) present in m-$ZrO_2$.[45] Increasing the reaction temperature from 350 °C to 400 °C only resulted in a small TOF enhancement, in agreement with previous reports.[68] Lifetime studies at 400 °C evidenced limited deactivation (<20 %) over 8.5 h on-stream in all cases (**Figure S8**). Deactivation may occur through site-blocking by strongly bound bidentate acetate species[47] and/or coke formation. Element analysis confirmed the presence of significant carbon post-reaction, whose content was inversely proportional to calcination temperature (falling from 8 to 1 wt% for $ZrO_2$(300) and $ZrO_2$(800) respectively), suggesting that strong acid sites present at the surface of t-$ZrO_2$ were responsible for unselective oligomerisation reactions. Although all catalysts exhibited similar decreases in their absolute conversion over the course of extended reaction, their relative deactivation was proportional to their carbon content post-reaction (**Figure S9**), confirming carbon deposition as responsible for deactivation. Powder XRD provided no evidence of sintering during ketonisation (**Figure S10**).

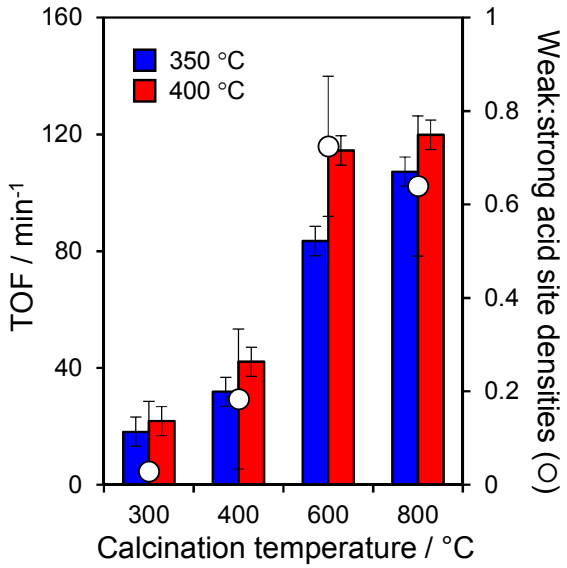


**Figure 4.** Correlation between TOFs (normalised per acid site) for acetic acid ketonisation at 50 % iso-conversion and weak:strong acid site densities for $Zr(OH)_4$ as a function of calcination temperature. Reaction conditions: 200 mg catalyst, 0.1-0.4 ml.min$^{-1}$ acetic acid, 50 ml.min$^{-1}$ $N_2$, and ambient pressure.

Acetone selectivity was only weakly-dependent on reaction temperature at ~32 % of the maximum theoretical value (**Figure S11**), however its production was directly proportional to the weak acid site density as shown in **Figure 5** at both reaction temperatures. The principal by-product from GC-MS was 1 2-propanediol 2-acetate (**Figure S1**), with only trace isobutene detected.

View Article Online
DOI: 10.1039/C7CY02541F




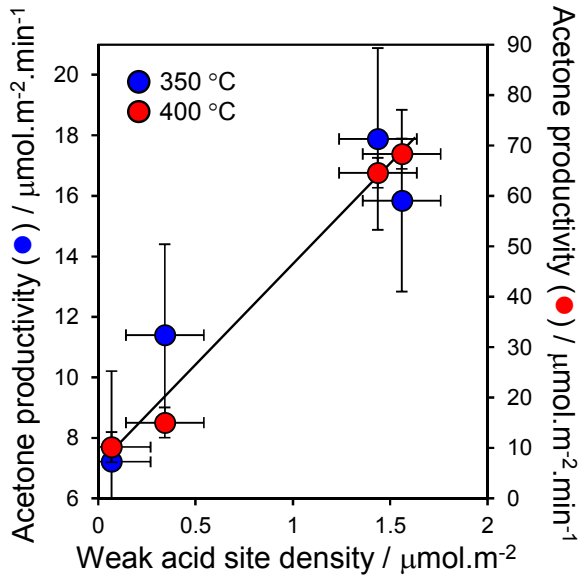


**Figure 5**. Acetone productivity from acetic acid ketonisation at 50 % ico-conversion for $Zr(OH)_4$ as a function of weak acid site density (calcination temperature). Reaction conditions: 200 mg catalyst, 0.1-0.4 ml.min$^{-1}$ acetic acid, 50 ml.min$^{-1}$ $N_2$, and ambient pressure.

Our observation that weak Lewis acid sites and/or related acid-base pairs are the active species responsible for acetic acid ketonisation to acetone in the vapour phase is consistent with previous experimental[69-72] and computational studies.[47] DFT calculations indicate that acetic acid may adopt several adsorption modes over zirconia shown in **Scheme 2**: molecular acetic acid (I); monodentate acetate (II); or as bridging, bidentate acetate (III).[47] Recent reports suggest that ketonisation preferentially proceeds via a reaction between molecular (I) and monodentate (II) species, bound at adjacent acid-base pairs. The development of high performance ketonisation catalysts therefore requires new synthetic routes to prepare (and stabilise) high area m-$ZrO_2$ nanoparticles, possessing higher densities of weak Lewis acid sites to enhance selectivity to acetone at lower reaction temperatures.

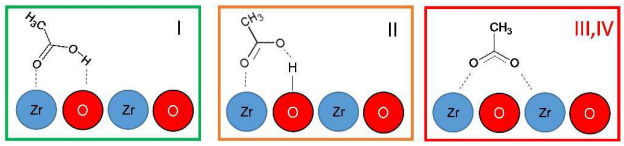


Scheme 2. Surface species formed upon adsorption of acetic acid on $ZrO_2$.

## Conclusions

The evolution of structural and acidic properties of zirconia nanocatalysts was therefore investigated as a function of calcination temperature to elucidate underlying structure-reactivity relations in acetic acid ketonisation. Powder XRD evidenced that calcination of amorphous $Zr(OH)_4$ resulted in the crystallisation of small (~9 nm) t-$ZrO_2$ particles at 400 °C, and a subsequent phase transition to larger (15-48 nm) monoclinic crystallites >600 °C, whose size increases with temperature. Pyridine titration showed that all zirconias were pure Lewis acids, however propylamine temperature-programmed desorption revealed that zirconia restructuring was accompanied by an increase in the surface density of Lewis acid sites, and concomitant decrease in their acid strength. The emergence of new, weak Lewis acid sites >300 °C correlates with surface dehydroxylation and anion vacancy formation observed by photoelectron spectroscopy. Turnover frequencies for vapour phase acetic acid ketonisation at 350 °C and 400 °C mirror the evolution of surface acidity, with acetone productivity directly proportional to the surface density of weak Lewis acid sites; the latter (or their resulting acid-base pairs) are therefore identified as the active catalytic species for ketonisation. Strong Lewis acid sites favour competing unselective reactions and carbon laydown, although <20 % deactivation was observed for 8.5 h on-stream in all cases, evidencing good stability for all calcined zirconias. Acetic acid ketonisation thus offers an attractive route to upgrade biomass-derived fast pyrolysis vapours through close-coupling of zirconia catalysts possessing high densities of weak Lewis acid sites and/or related acid-base pairs to the hot outlet of a pyrolysis reactor.

## Acknowledgements

We thank the EPSRC (EP/K036548/2, EP/K014676/1, EP/N009924/1) for financial support. K.W. thanks the Royal Society for the award of an Industry Fellowship. The work was also conducted with support from the EU under the frame of the FP7-funded CAScade deoxygenation process using tailored nanoCATalysts for the production of BiofuELs from lignocellullosic biomass (CASCATBEL) project (Grant Agreement No. 604307). MEL Chemicals are thanked for the provision of $Zr(OH)_4$.

## Notes and references

1. M. Z. Jacobson, *Energy & Environmental Science*, 2009, **2**, 148-173.
2. K. Wilson and A. F. Lee, *Phil. Trans. R. Soc. A*, 2016, **374**, 20150081.
3. D. M. Alonso, J. Q. Bond and J. A. Dumesic, *Green Chemistry*, 2010, **12**, 1493-1513.
4. W. Leitner, J. Klankermayer, S. Pischinger, H. Pitsch and K. Kohse-Höinghaus, *Angewandte Chemie International Edition*, 2017, **56**, 5412-5452.
5. A. V. Bridgwater, *Biomass Bioenerg*, 2012, **38**, 68-94.
6. A. V. Bridgwater, *Environ Prog Sustain*, 2012, **31**, 261-268.
7. S. S. Toor, L. Rosendahl and A. Rudolf, *Energy*, 2011, **36**, 2328-2342.
8. D. C. Elliott, P. Biller, A. B. Ross, A. J. Schmidt and S. B. Jones, *Bioresource Technology*, 2015, **178**, 147-156.
9. M. M. Yung, W. S. Jablonski and K. A. Magrini-Bair, *Energy & Fuels*, 2009, **23**, 1874-1887.

View Article Online
DOI: 10.1039/C7CY02541F




10. H. Jahangiri, J. Bennett, P. Mahjoubi, K. Wilson and S. Gu, *Catal Sci Technol*, 2014, **4**, 2210-2229.
11. S. Sartipi, M. Makkee, F. Kapteijn and J. Gascon, *Catal Sci Technol*, 2014, **4**, 893-907.
12. T. Sfetsas, C. Michailof, A. Lappas, Q. Li and B. Kneale, *Journal of Chromatography A*, 2011, **1218**, 3317-3325.
13. L. Ciddor, J. A. Bennett, J. A. Hunns, K. Wilson and A. F. Lee, *Journal of Chemical Technology & Biotechnology*, 2015, **90**, 780-795.
14. J. A. Bennett, C. M. A. Parlett, M. A. Isaacs, L. J. Durndell, L. Olivi, A. F. Lee and K. Wilson, *ChemCatChem*, 2017, **9**, 1648-1654.
15. T. N. Pham, D. Shi and D. E. Resasco, *Topics in Catalysis*, 2014, **57**, 706-714.
16. E. Heracleous, D. Gu, F. Schüth, J. A. Bennett, M. A. Isaacs, A. F. Lee, K. Wilson and A. A. Lappas, *Biomass Conversion and Biorefinery*, 2017, **7**, 319-329.
17. A. Osatiashtiani, B. Puértolas, C. C. S. Oliveira, J. C. Manayil, B. Barbero, M. Isaacs, C. Michailof, E. Heracleous, J. Pérez-Ramírez, A. F. Lee and K. Wilson, *Biomass Conversion and Biorefinery*, 2017, **7**, 331-342.
18. J. C. Manayil, A. Osatiashtiani, A. Mendoza, C. M. A. Parlett, M. A. Isaacs, L. J. Durndell, C. Michailof, E. Heracleous, A. Lappas, A. F. Lee and K. Wilson, *ChemSusChem*, **10**, 3506-3511.
19. J. C. Manayil, C. V. M. Inocencio, A. F. Lee and K. Wilson, *Green Chemistry*, 2016, **18**, 1387-1394.
20. T. N. Pham, T. Sooknoi, S. P. Crossley and D. E. Resasco, *Acs Catal*, 2013, **3**, 2456-2473.
21. C. A. Gaertner, J. C. Serrano-Ruiz, D. J. Braden and J. A. Dumesic, *Industrial & Engineering Chemistry Research*, 2010, **49**, 6027-6033.
22. , Google Patents, 1938.
23. O. Nagashima, S. Sato, R. Takahashi and T. Sodesawa, *Journal of Molecular Catalysis A: Chemical*, 2005, **227**, 231-239.
24. R. Pestman, R. M. Koster, A. vanDuijne, J. A. Z. Pieterse and V. Ponec, *J Catal*, 1997, **168**, 265-272.
25. S. D. Randery, J. S. Warren and K. M. Dooley, *Appl Catal a-Gen*, 2002, **226**, 265-280.
26. K. M. Dooley, A. K. Bhat, C. P. Plaisance and A. D. Roy, *Appl Catal a-Gen*, 2007, **320**, 122-133.
27. M. Gliński and J. Kijeński, *Reaction Kinetics and Catalysis Letters*, 2000, **69**, 123-128.
28. K. M. Parida, A. Samal and N. N. Das, *Applied Catalysis A: General*, 1998, **166**, 201-205.
29. R. Martinez, M. C. Huff and M. A. Barteau, *J Catal*, 2004, **222**, 404-409.
30. K. S. Kim and M. A. Barteau, *J Catal*, 1990, **125**, 353-375.
31. R. Pestman, R. M. Koster, J. A. Z. Pieterse and V. Ponec, *J Catal*, 1997, **168**, 255-264.
32. M. Gliński and J. Kijeński, *Applied Catalysis A: General*, 2000, **190**, 87-91.
33. K. Okumura and Y. Iwasawa, *J Catal*, 1996, **164**, 440-448.
34. S. S. Kistler, S. Swann and E. G. Appel, *Industrial & Engineering Chemistry*, 1934, **26**, 388-391.
35. J. Das and K. Parida, *Reaction Kinetics and Catalysis Letters*, 2000, **69**, 223-229.
36. K. Parida and J. Das, *Journal of Molecular Catalysis A: Chemical*, 2000, **151**, 185-192.
37. M. Glinski and J. Kijenski, *Appl Catal a-Gen*, 2000, **190**, 87-91.
38. M. I. Zaki, M. A. Hasan and L. Pasupulety, *Langmuir*, 2001, **17**, 768-774.
39. M. I. Zaki, M. A. Hasan, F. A. Al-Sagheer and L. Pasupulety, *Colloid Surface A*, 2001, **190**, 261-274.
40. K. Parida and H. K. Mishra, *Journal of Molecular Catalysis A: Chemical*, 1999, **139**, 73-80.
41. K. C. Patil, G. V. Chandrashekhar, M. V. George and C. N. R. Rao, *Canadian Journal of Chemistry*, 1968, **46**, 257-265.
42. A. V. Ignatchenko and E. I. Kozliak, *Acs Catal*, 2012, **2**, 1555-1562.
43. Y. Yamada, M. Segawa, F. Sato, T. Kojima and S. Sato, *Journal of Molecular Catalysis A: Chemical*, 2011, **346**, 79-86.
44. G. Pacchioni, *Acs Catal*, 2014, **4**, 2874-2888.
45. S. Wang and E. Iglesia, *J Catal*, 2017, **345**, 183-206.
46. S. Tosoni and G. Pacchioni, *J Catal*, 2016, **344**, 465-473.
47. S. Wang and E. Iglesia, *The Journal of Physical Chemistry C*, 2017, **121**, 18030-18046.
48. H.-Y. T. Chen, S. Tosoni and G. Pacchioni, *Surface Science*, 2016, **652**, 163-171.
49. M. A. Hasan, M. I. Zaki and L. Pasupulety, *Applied Catalysis A: General*, 2003, **243**, 81-92.
50. A. Osatiashtiani, A. F. Lee, D. R. Brown, J. A. Melero, G. Morales and K. Wilson, *Catal Sci Technol*, 2014, **4**, 333-342.
51. T. Chraska, A. H. King and C. C. Berndt, *Materials Science and Engineering: A*, 2000, **286**, 169-178.
52. V. N. Panchenko, Y. A. Zaytseva, M. N. Simonov, I. L. Simakova and E. A. Paukshtis, *Journal of Molecular Catalysis A: Chemical*, 2014, **388**, 133-140.
53. R. Brenier, J. Mugnier and E. Mirica, *Appl Surf Sci*, 1999, **143**, 85-91.
54. M. Hino, M. Kurashige, H. Matsuhashi and K. Arata, *Thermochim Acta*, 2006, **441**, 35-41.
55. S. Tsunekawa, K. Asami, S. Ito, M. Yashima and T. Sugimoto, *Appl Surf Sci*, 2005, **252**, 1651-1656.
56. M. C. Deibert and R. Kahraman, *Appl Surf Sci*, 1989, **37**, 327-336.
57. L. Soriano, M. Abbate, J. Faber, C. Morant and J. M. Sanz, *Solid State Communications*, 1995, **93**, 659-665.
58. S.-m. Chang and R.-a. Doong, *Chemistry of Materials*, 2007, **19**, 4804-4810.
59. S.-m. Chang and R.-a. Doong, *Chemistry of Materials*, 2005, **17**, 4837-4844.
60. Y. Lee, J.-W. Choi, D. J. Suh, J.-M. Ha and C.-H. Lee, *Applied Catalysis A: General*, 2015, **506**, 288-293.
61. H. M. Altass and A. E. R. S. Khder, *Journal of Molecular Catalysis A: Chemical*, 2016, **411**, 138-145.
62. C. Morterra, G. Cerrato, L. Ferroni, A. Negro and L. Montanaro, *Appl Surf Sci*, 1993, **65**, 257-264.
63. H.-J. Eom, M.-S. Kim, D.-W. Lee, Y.-K. Hong, G. Jeong and K.-Y. Lee, *Applied Catalysis A: General*, 2015, **493**, 149-157.
64. K. T. Jung and A. T. Bell, *Journal of Molecular Catalysis A: Chemical*, 2000, **163**, 27-42.
65. S. Makoto, T. Kyoko, K. Hideyuki and M. Hajime, *Bulletin of the Chemical Society of Japan*, 1990, **63**, 258-259.

View Article Online
DOI: 10.1039/C7CY02541F


66. K. Pokrovski, K. T. Jung and A. T. Bell, *Langmuir*, 2001, **17**, 4297-4303.
67. V. Bolis, C. Morterra, M. Volante, L. Orio and B. Fubini, *Langmuir*, 1990, **6**, 695-701.
68. A. Pulido, B. Oliver-Tomas, M. Renz, M. Boronat and A. Corma, *ChemSusChem*, 2013, **6**, 141-151.
69. A. Mattsson and L. Österlund, *The Journal of Physical Chemistry C*, 2010, **114**, 14121-14132.
70. Q. Ma, Y. Liu, C. Liu and H. He, *Physical Chemistry Chemical Physics*, 2012, **14**, 8403-8409.
71. E. Finocchio, R. J. Willey, G. Busca and V. Lorenzelli, *Journal of the Chemical Society, Faraday Transactions*, 1997, **93**, 175-180.
72. A. C. Geiculescu and H. G. Spencer, *Journal of Sol-Gel Science and Technology*, 2000, **17**, 25-35.

View Article Online
DOI: 10.1039/C7CY02541F



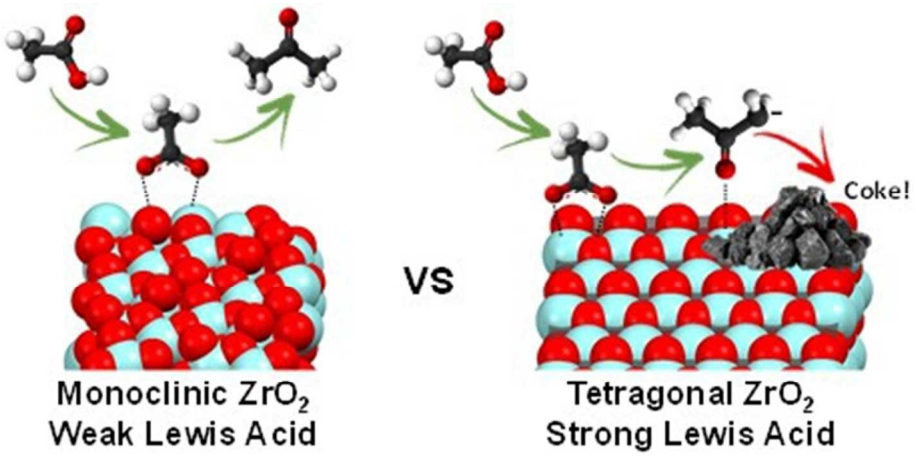


78x39mm (150 x 150 DPI)